Advanced Steel Construction – Vol. 19 No. 3 (2023) 197–208
DOI:10.18057/IJASC.2023.19.3.2

DEVELOPMENT OF ANALYTICAL MODELS FOR PREDICTING THE FLEXURAL BEHAVIOUR OF ENGINEERED CEMENTITIOUS COMPOSITES – HIGH STRENGTH STEEL COMPOSITE BEAMS

Cong-Luyen Nguyen [1, *] and Chi-King Lee [2]

[1] *The University of Danang – University of Science and Technology, Danang 550000, Vietnam*
[2] *School of Engineering and Information Technology, The University of New South Wales, Canberra, ACT 2600, Australia*
** (Corresponding author: E-mail: ncluyen@dut.udn.vn)*

ABSTRACT

This paper presents the results of three-dimensional (3D) finite element (FE) and analytical models on the prediction of the flexural behaviour of composite beams comprising high strength steel (HSS) I-section and Engineered Cementitious Composite (ECC) slab. In the FE approach, 108 composite beam models which cover a wide range of key parameters including HSS grade, ECC compressive strength, HSS section depth, ECC slab thickness, ECC slab width were generated and analysed. The flexural strength of these composite beam models was subsequently employed to validate the accuracies of some commonly used flexural strength prediction methods that are originally based on the rigid plastic analysis (RPA). It was found that these methods generally underpredicted the flexural strength of the ECC-HSS composite beams. Hence, a simple analytical model was proposed, and validation results of its accuracy showed that this simple analytical model produced more accurate predictions than the RPA methods. In order to allow designers to obtain the load-deflection curves of the beams, a full analytical model which is based on strain compatibility and force equilibrium was also developed. Validations against both FE model and test results showed that this full analytical model produced the most accurate flexural strength predictions.

ARTICLE HISTORY

Received: 26 September 2022
Revised: 16 February 2023
Accepted: 23 February 2023

KEYWORDS

Engineered cementitious Composite–high strength steel composite beams;
Flexural behaviour;
Flexural strength;
Rigid plastic analysis;
Simple analytical model;
Full analytical model

1. Introduction

High strength steel (HSS), which normally possesses yield strength of higher than 690 MPa, has been increasingly applied in structural engineering thank to its superior strength to weight ratio which enhances structural performance and leads to more sustainable design. Furthermore, advances in steel manufacturing technology also reduce the cost of HSS and increase its weldability. As a result, many studies have been dedicated in an attempt to investigate the behaviour of HSS structures in forms of bare steel structures [1-8], composite columns [9-11], connection details [12-14], encased [15-17] and composite beams [18-22].

One potential application of HSS is the construction of composite beam in which the HSS section is placed at the bottom to resist tension and normal strength concrete (NSC) is placed on top to resist compression. Nevertheless, previous studies reported that the superior yield strength of HSS section might not be fully utilized when NSC slab was used. To be more specific, the yield strain of HSS (0.35% for S690 grade) could exceed the peak compressive strain (≈0.3%) of NSC. As a result, this may lead to a premature failure of NSC-HSS composite beam when NSC slab is crushed before the HSS section is fully yielded [19-24]. When comparing the FE and test results of NSC-HSS composite beams with predicted results by the rigid plastic analysis (RPA) in terms of its flexural strength, it was found that the RPA overpredicted their test results. Note that RPA approach assumes HSS section fully yielded in its calculation of flexural strength and has been adopted by many national standards to predict the flexural strength of NSC–normal strength steel (NSS) composite beams [25,26].

In order to address such strain incompatibility issue, Engineered Cementitious Composites (ECC) was employed to replace NSC in constructing slab of HSS composite beam [18]. ECC is a form of advanced building material [27] which is well-known for its high compressive and tensile strain capacities [17,28]. The compressive strain at peak strength for almost all types of ECC exceed 0.5% which is higher than the yield strain of nearly all HSS grades employing in structural engineering. This allows ECC to work efficiently with HSS in composite beam construction. In addition, it is recently reported that ECC is capable of preventing longitudinal shear failure of composite beam if NSC slab is used in conjunction with HSS section [29]. By conducting a series of test on ECC-HSS composite beams, Nguyen and Lee [18] found that ECC-HSS composite beams showed higher strength and ductility than those constructed with NSC slab and HSS I-section. In addition, the RPA conservatively predicted the flexural strength of ECC-HSS composite beams [18]. Nevertheless, limited results obtained from the costly and time-consuming experimental study are obviously not sufficient to examine the prediction of RPA methods over the flexural capacity of ECC-HSS composite beams. Thus, in this study, the 3D FE model which has been developed and validated against the experimental results reported in authors' previous work [18] was employed to generate 108 models which cover a wide range of key parameters of the composite beams. The results of these models were then used to assess the accuracies of flexural strength predictions obtained from different methods based on RPA. Simple analytical model was subsequently developed in order to predict the flexural strength of ECC-HSS composite beams more precisely. Furthermore, a full analytical model was proposed to allow engineers to obtain the ECC-HSS composite beam's detailed responses (i.e., the load-displacement curves, flexural strength).

2. FE model used and parameter design

The FE model employed in this study, which uses the FE software ABAQUS [30], was shown to produce accurate predictions when comparing with experimental results [18] for all stages of the composite beams comprising ECC slab and HSS section under 4-point bending load. As the model development and validation processes were described with details in [18], only a summary of its key features is given here.

2.1. Key features of the FE model used

The beam cross-sectional configuration is shown in Fig. 1(a). All beams modelled are simply supported with clear span of 3100 mm and are under four-point bending. The lengths of the pure bending region and the shear span are 800 mm and 1150 mm, respectively [18]. The main structural components of the composite beam which consist of the HSS section, the ECC slab and the shear studs were modelled using eight-node hexahedral solid elements with reduced integration (C3D8R) [30]. Four-node shell elements (S4R) and three-node truss elements (T3D2) were employed to model the profiled steel sheeting (PSS) and slab reinforcement, respectively. After a mesh size sensitivity analysis [18], nominal element sizes of 40 mm and 20 mm were respectively used within the two shear spans and pure bending region. Interactions between PSS and ECC slab, between PSS and HSS section, and between shear studs and ECC slab were defined by ABAQUS's surface-to-surface contact feature. Contacts between shear studs and HSS section's top flange, between loading plates and the slab were guaranteed by tie constraints (Fig. 1(b)). Roller and pin constraints were employed to reproduce the test support conditions. Loading was applied in such a way that prescribed downward displacement was assigned to nodes located on the surfaces of two loading plates. A typical FE model is shown in Fig. 1(c). Constitutive models for different materials used were

presented in [18] and are indicated in Fig. 2(a)-(f). For ECC, damage evolution was applied when it reached its compressive strain, as indicated in Fig. 2(g). Values of all key material parameters employed in the constitutive models of the FE models are listed in Tables 1–2.

2.2. Parameter design

The following five key parameters which define the beam's cross-sectional dimensions and material properties are considered and their modelling ranges are listed below:

(1) HSS grade (S690 and S960 grades HSS)
(2) ECC compressive strength (40 MPa and 70 MPa)
(3) HSS section depth (180 mm, 230 mm and 280 mm)
(4) ECC slab thickness (140 mm, 170 mm and 200 mm)
(5) ECC slab width (600 mm, 1000 mm and 1400 mm).

Names of composite beams modelled are labelled using the format of "SW*a*-ST*b*-ID*c*-E*x*-S*y*" where "SW", "ST", "ID" respectively denotes the ECC slab width, ECC slab thickness and depth of HSS I-section (Fig. 1(a)). "E" and "S" represent the compressive strength of ECC (f'_{ECC}) and the HSS yield strength ($f_{y(HSS)}$), respectively. "*a*", "*b*", "*c*" are respectively the slab width, slab thickness and HSS section depth in mm. "*x*", "*y*" are f'_{ECC} and $f_{y(HSS)}$ in MPa, respectively. For instance, "SW600-ST140-ID180-E40-S690" refers to a beam comprising a 600 mm × 140 mm ECC slab with compressive strength of 40 MPa connected to a S690 HSS section with a depth of 180 mm. These beams were arranged with the same shear studs with shank diameter of 19 mm and stud height of 100 mm after welding, stud spacing of 100 mm, steel beam's flange width b_f of 120 mm, steel beam's flange thickness t_f of 8 mm, and steel beam's web thickness t_w of 6 mm. These were similar to the test conducted by the authors reported in [18]. It should be noted that shear connection degree η of the beam is defined by the ratio of the number of shear connectors installed in the beam (n) to the number of shear connectors required for full shear connection (n_f). Beam with $\eta \geq 1$ is considered as fully connected in shear. Otherwise, it is partially shear connected. η is affected by all of parameters mentioned above since they all have effects on the value of n_f. As the shear stud spacing was kept constant at 100 mm (n is constant) but cross-sectional dimensions and material parameters are varied among the beams (n_f is varied), η for these sets of models varied between 0.42 and 0.82. These models were divided into two subsets based on the HSS yield strength (i.e, S690 MPa and S960 MPa). Their details and flexural strength (P_{FE}) obtained from the FE modelling are listed in Table 3.

3. Comparing flexural strength obtained from FE models with RPA predictions

The RPA [31] is a reliable method in predicting the flexural strength of composite beams constructing by using NSC slab and NSS section. It uses the concept of stress blocks for the calculation of the beam's flexural strength. It has been adopted by Eurocode 4 [25] and AS2327 [26] for NSC-NSS composite beam design. However, previous studies [19-21,23] reported that the flexural strength predicted by RPA ($M_{RPA,equi}$) might not be conservative for NSC-HSS composite beams. One possible reason is that the NSC slab was crushed before the HSS section reached a high degree of yielding [18]. For NSC-HSS beam, Eurocode 4 [25] and AS2327 [26] suggest that when using the RPA, a reduction factor should be applied to account for the limited strain hardening of HSS. Hence, the flexural strength predicted by these codes, $M_{EC4/AS2327}$, is more conservative than $M_{RPA,equi}$.

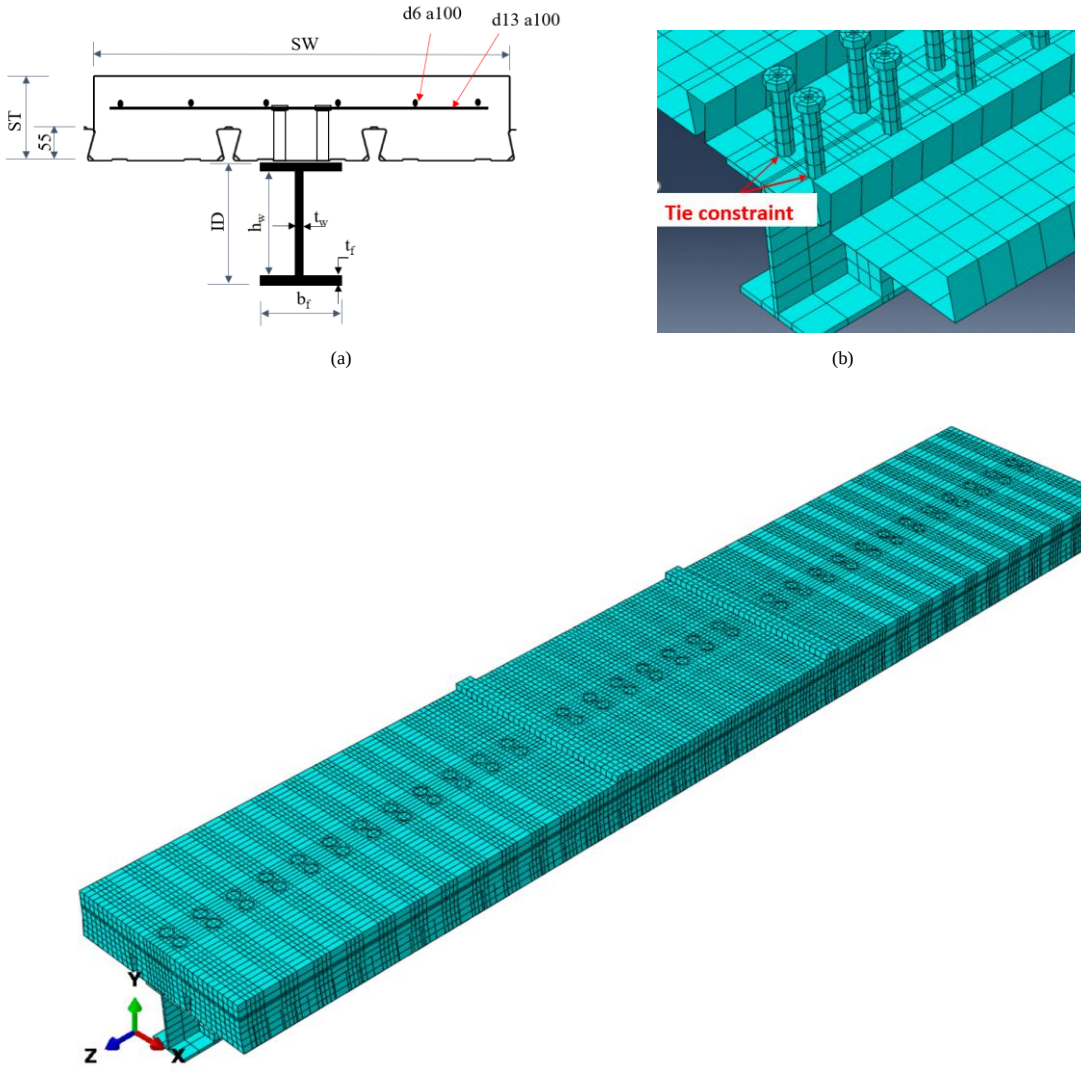

(a) (b)

(c)

Fig. 1 Beam's cross-section and FE model: (a) Cross-section configuration; (b) Shear studs meshing and contact between shear studs and steel beam; (c) Typical FE model

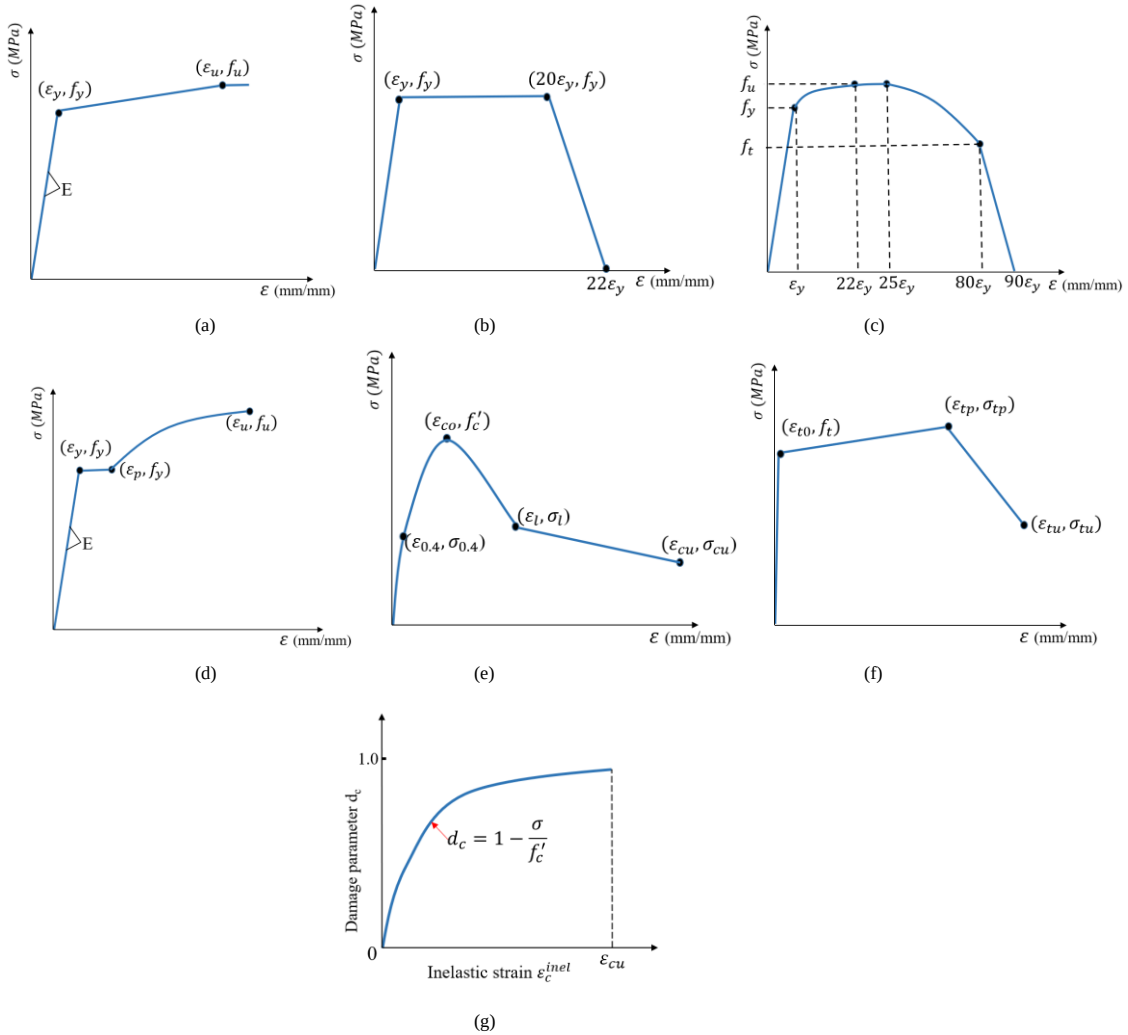

Fig. 2 Stress – strain models for materials used in the FE models: (a) HSS; (b) PSS; (c) Headed shear stud; (d) Steel reinforcement; (e) Compressive stress-strain model for ECC; (f) Tensile stress-strain model for ECC; (g) Compressive damage model for ECC

Table 1
Material properties used in the FE models

Material	E (GPa)	ε_y(%)	f_y (MPa)	ε_p(%)	ε_u(%)	f_u (MPa)	f_t (MPa)
S690	200	0.35	690	-	8.0	770	-
S960	200	0.48	960	-	5.5	980	-
Steel reinforcement	200	0.27	543	2.4	20.8	632	-
PSS	248	0.28	691	-	-	-	-
Headed shear stud	200	0.17	344	-	-	410	331

Table 2
Material properties of ECC used in the FE models

Material	E_c (GPa)	$\sigma_{0.4}$ (MPa)	$\varepsilon_{0.4}$ (%)	f'_c (MPa)	ε_{co} (%)	σ_l (MPa)	ε_l (%)	σ_{cu} (MPa)	ε_{cu} (%)	f_t (MPa)	ε_{to} (%)	σ_{tp} (MPa)	ε_{tp} (%)	σ_{tu} (MPa)	ε_{tu} (%)
ECC40	15.5	16	0.10	40	0.50	20.0	0.85	10.0	1.20	2.43	0.016	3.2	1.2	1.7	2.2
ECC70	20.5	28	0.14	70	0.53	30.0	0.95	13.5	1.40	4.40	0.021	5.3	1.0	3.0	1.7

Table 3
FE model details and their flexural strength

HSS S690 Beams (54 models)				HSS S960 Beams (54 models)			
Main dimensions	Materials	η	P_{FE} (kN)	Main dimensions	Materials	η	P_{FE} (kN)
SW600-ST140-ID180	E40-S690	0.82	604	SW600-ST140-ID180	E40-S960	0.82	712
	E70-S690	0.82	700		E70-S960	0.59	828
SW600-ST140-ID230	E40-S690	0.82	734	SW600-ST140-ID230	E40-S960	0.82	876
	E70-S690	0.74	835		E70-S960	0.54	1001
SW600-ST140-ID280	E40-S690	0.82	890	SW600-ST140-ID280	E40-S960	0.82	1014

	E70-S690	0.68	994		E70-S960	0.54	1215
SW600-ST170-ID180	E40-S690	0.71	676	SW600-ST170-ID180	E40-S960	0.61	767
	E70-S690	0.82	815		E70-S960	0.59	920
SW600-ST170-ID230	E40-S690	0.64	813	SW600-ST170-ID230	E40-S960	0.61	937
	E70-S690	0.74	955		E70-S960	0.53	1098
SW600-ST170-ID280	E40-S690	0.61	962	SW600-ST170-ID280	E40-S960	0.61	1122
	E70-S690	0.68	1110		E70-S960	0.49	1294
SW600-ST200-ID180	E40-S690	0.71	766	SW600-ST200-ID180	E40-S960	0.51	853
	E70-S690	0.82	931		E70-S960	0.59	1030
SW600-ST200-ID230	E40-S690	0.64	916	SW600-ST200-ID230	E40-S960	0.48	1038
	E70-S690	0.74	1095		E70-S960	0.53	1241
SW600-ST200-ID280	E40-S690	0.59	1044	SW600-ST200-ID280	E40-S960	0.48	1185
	E70-S690	0.68	1244		E70-S960	0.49	1395
SW1000-ST140-ID180	E40-S690	0.71	672	SW1000-ST140-ID180	E40-S960	0.51	773
	E70-S690	0.82	798		E70-S960	0.59	908
SW1000-ST140-ID230	E40-S690	0.64	819	SW1000-ST140-ID230	E40-S960	0.49	965
	E70-S690	0.74	963		E70-S960	0.53	1112
SW1000-ST140-ID280	E40-S690	0.59	975	SW1000-ST140-ID280	E40-S960	0.49	1166
	E70-S690	0.68	1106		E70-S960	0.49	1320
SW1000-ST170-ID180	E40-S690	0.71	781	SW1000-ST170-ID180	E40-S960	0.51	876
	E70-S690	0.82	947		E70-S960	0.59	1045
SW1000-ST170-ID230	E40-S690	0.65	923	SW1000-ST170-ID230	E40-S960	0.46	1038
	E70-S690	0.74	1093		E70-S960	0.53	1242
SW1000-ST170-ID280	E40-S690	0.59	1087	SW1000-ST170-ID280	E40-S960	0.42	1288
	E70-S690	0.68	1256		E70-S960	0.49	1452
SW1000-ST200-ID180	E40-S690	0.71	906	SW1000-ST200-ID180	E40-S960	0.51	994
	E70-S690	0.82	1107		E70-S960	0.59	1203
SW1000-ST200-ID230	E40-S690	0.65	1048	SW1000-ST200-ID230	E40-S960	0.46	1171
	E70-S690	0.74	1253		E70-S960	0.53	1393
SW1000-ST200-ID280	E40-S690	0.59	1205	SW1000-ST200-ID280	E40-S960	0.42	1371
	E70-S690	0.68	1418		E70-S960	0.49	1604
SW1400-ST140-ID180	E40-S690	0.71	759	SW1400-ST140-ID180	E40-S960	0.51	841
	E70-S690	0.82	906		E70-S960	0.59	1028
SW1400-ST140-ID230	E40-S690	0.65	894	SW1400-ST140-ID230	E40-S960	0.46	1042
	E70-S690	0.74	1043		E70-S960	0.53	1208
SW1400-ST140-ID280	E40-S690	0.59	1045	SW1400-ST140-ID280	E40-S960	0.42	1238
	E70-S690	0.68	1196		E70-S960	0.49	1406
SW1400-ST170-ID180	E40-S690	0.71	894	SW1400-ST170-ID180	E40-S960	0.51	998
	E70-S690	0.82	1083		E70-S960	0.59	1210
SW1400-ST170-ID230	E40-S690	0.65	1054	SW1400-ST170-ID230	E40-S960	0.46	1219
	E70-S690	0.74	1251		E70-S960	0.53	1405
SW1400-ST170-ID280	E40-S690	0.59	1208	SW1400-ST170-ID280	E40-S960	0.42	1420
	E70-S690	0.68	1415		E70-S960	0.49	1613
SW1400-ST200-ID180	E40-S690	0.71	1075	SW1400-ST200-ID180	E40-S960	0.51	1229
	E70-S690	0.82	1341		E70-S960	0.59	1457
SW1400-ST200-ID230	E40-S690	0.65	1214	SW1400-ST200-ID230	E40-S960	0.46	1338
	E70-S690	0.74	1520		E70-S960	0.53	1699
SW1400-ST200-ID280	E40-S690	0.59	1369	SW1400-ST200-ID280	E40-S960	0.42	1540
	E70-S690	0.68	1655		E70-S960	0.49	1861

For partially shear connected beams, due to the slip strain between the steel section and the slab, stress blocks of the beam will be more complicated and more complex calculation is needed to obtain $M_{RPA,equi}$. In this case, Eurocode 4 [25] adopts the following simplified method for partially shear connected beams so that

$$M_{RPA,sim} = M_{pl,a} + \eta(M_{pl,Rd} - M_{pl,a}) \quad (1)$$

In Eqn. (1), $M_{RPA,sim}$ is the flexural strength predicted by the simplified method, $M_{pl,a}$ is the moment resistance of HSS section alone while $M_{pl,Rd}$ is the

moment resistance for fully shear connected beam. In Eqn. (1), the maximum value of η is 1.0. $M_{RPA,sim}$ generally gives a more conservative prediction than $M_{RPA,equi}$.

Experimental results obtained by the authors [18] showed that when ECC with high compressive strain (>0.5%) was employed to replace NSC, the HSS section could develop a higher degree of yielding before the ECC slab was crushed. Hence, in order to study the accuracy of different prediction approaches mentioned above for a wider range of ECC-HSS composite beams, the flexural strength M_{FE} obtained from the 108 models were compared with the predictions from $M_{RPA,equi}$, $M_{RPA,sim}$ and $M_{EC4/AS2327}$.

Means and standard deviations of the ratios $M_{FE/MRPA,sim}$, $M_{FE}/M_{RPA,equi}$ and $M_{FE}/M_{EC4/AS2327}$ for all beams modelled obtained are summarized in Table 4. Fig. 3 plots the ratio $M_{FE}/M_{RPA,sim}$ against η. Fig. 3 and Table 4 show that predictions by $M_{RPA,sim}$ were more conservative than the FE predictions, even for S960 HSS section beams. On average, $M_{RPA,sim}$ overpredicted the flexural strength of the beams by 28%. The main reasons were (i) ECC was employed to replace NSC, a high degree of yielding of the HSS was achieved and (ii) the more conservative Eqn. (1) was used.

The ratio $M_{FE}/M_{RPA,equi}$ obtained for the 108 ECC-HSS beams modelled together with the experimental results obtained for ECC/NSC-HSS beams tested in [18] and those NSC-HSS beams reported in [21] and [23] are plotted in Fig. 4. Again, $M_{FE}/M_{RPA,equi}$ of most ECC-HSS beams were above unity with an average value of 1.17. This ratio is 11% lower than the average ratio for $M_{FE}/M_{RPA,sim}$ since $M_{RPA,equi}$ uses a more realistic/detailed stress block distribution for calculation. This confirmed that for most ECC-HSS beams, a high degree of yielding of the HSS section was achieved. Moreover, Fig. 4 shows that for most NSC-HSS beams studied in [18,21,23] their ratios $M_{FE}/M_{RPA,equi}$ were less than unity, especially for beams with higher η values. This reconfirmed that the RPA failed to produce conservative prediction for NSC-HSS beams, especially when shear stress was effectively transferred and produced a higher compressive strain at the top NSC slab surfaces. For $M_{FE}/M_{EC4/AS2327}$, as $M_{EC4/AS2327}$ is obtained by reducing the values of $M_{RPA,equi}$, Fig. 5 and Table 4 show that an even more conservative prediction with a mean value of 1.38 was obtained.

4. Simple analytical model for flexural strength prediction of ECC-HSS composite beams

As it is found that $M_{RPA,equi}$, $M_{RPA,sim}$ and $M_{EC4/AS2327}$ generally underpredicted the flexural strength of ECC-HSS composite beams, in order to improve the prediction accuracy, a simple analytical model which is based on the RPA method and the following assumptions is developed:

(i) There is no shear failure nor shear lag.

(ii) All contributions of ECC parts in the PSS troughs are ignored.

(iii) As ECC slab reinforcement bars provided little flexural resistance while the PPS is thin and slip between the PPS and ECC were observed before the crushing of ECC [18], their contributions are ignored.

(iv) Full compressive strength of f'_{ECC} is developed within the effective areas of the ECC slab.

The stress distributions at the beam's ultimate states corresponding to full or partial shear connection are shown in Fig. 6. Expressions of internal forces of different components are summarized in Table 5. For full shear connection, three different cases corresponding to PNA within the ECC slab, within the steel flange and within the steel web can be identified. For partial shear connection, due to bond slip, only two cases corresponding to PNA within the steel flange and within the steel web are possible. Based on Fig. 6 and Table 5, a flow chart (Fig. 7) was developed for the calculation of the flexural strength obtained by simple analytical model M_{sana}. This simple analytical method was then applied to predict the flexural strength for the 108 beams generated from FE model. They were compared with the FE modelling results M_{FE} and the three test results obtained in [18]. A summary of the comparison results obtained given in Table 6 shows that the proposed simple analytical model provided more accurate but conservative predictions (on average 13%).

5. Full analytical model for predicting of flexural behaviour of ECC-HSS composite beams

5.1. Development of full analytical model

While the simple analytical model allows engineers to obtain a quick and more accurate prediction of the flexural strength of the beam over RPA approaches, it does not produce the load – displacement curve nor allows engineers to gain more insight into the flexural behaviour of the ECC-HSS composite beams at various stages before final failure. Hence, in this section, a full analytical model is developed which allows engineers to obtain detailed behaviours the composite beams without the need to conduct any time-consuming FE modelling. This analytical model is applicable for composite beams with HSS section connected with top ECC slab in forms of either solid slab or slab with PSS.

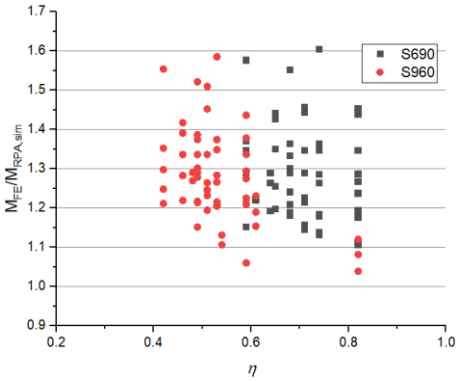

Fig. 3 $M_{FE}/M_{RPA,sim}$ versus shear connection degree for all FE modelled beams

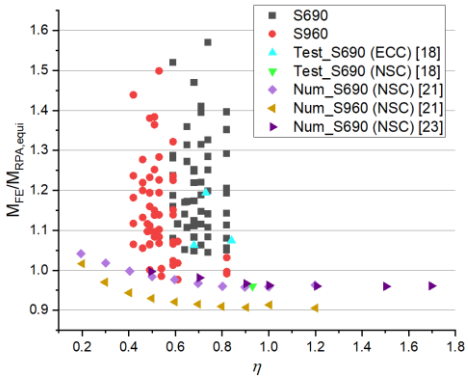

Fig. 4 $M_{FE}/M_{RPA,equi}$ obtained from all FE modelled beams and other studies [18,21,23] versus shear connection degree

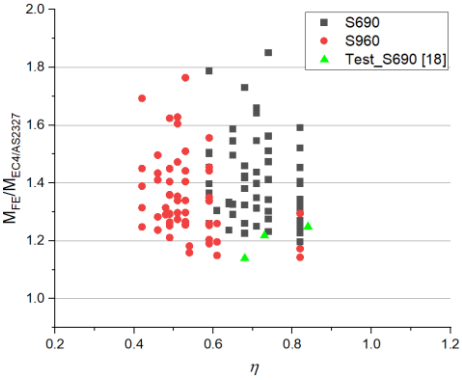

Fig. 5 $M_{FE}/M_{EC4/AS2327}$ versus shear connection degree for all FE modelled beams and experimental results from [18]

Table 4
Summary of comparison of flexural strength predictions obtained by FE model with RPA methods and EC4/AS2327

Beam group	$M_{FE}/M_{RPA,sim}$		$M_{FE}/M_{RPA,equi}$		$M_{FE}/M_{EC4/AS2327}$	
	Mean	SD	Mean	SD	Mean	SD
HSS S690 Beams (54 beams)	1.28	0.12	1.20	0.13	1.41	0.15
HSS S960 Beams (54 beams)	1.28	0.12	1.15	0.12	1.35	0.14
Overall (108 beams)	**1.28**	**0.12**	**1.17**	**0.13**	**1.38**	**0.15**

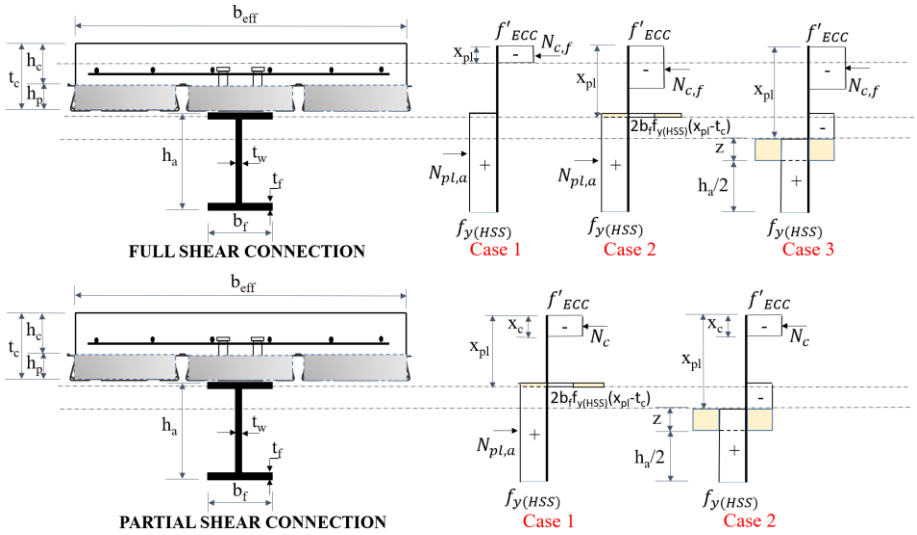

Fig. 6 Simple analytical model for calculating flexural strength of ECC-HSS composite beams

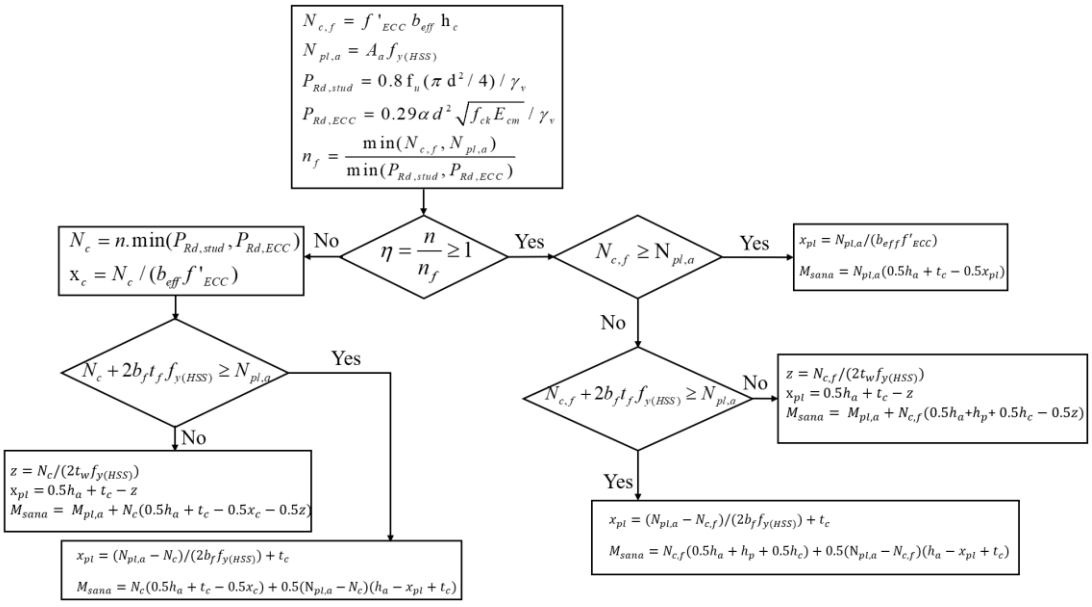

Fig. 7 Flow chart to calculate flexural strength of ECC-HSS composite beams using the simple analytical model

Table 5
Expressions for flexural strength prediction of ECC-HSS composite beams using the simple analytical model

Type of shear connection	Case		Analytical expression
Full	Case 1 (PNA in slab)	Depth of PNA	$x_{pl} = N_{pl,a} / (b_{eff} f'_{ECC})$
		Ultimate moment M_{sana}	$M_{sana} = N_{pl,a}(0.5h_a + t_c - 0.5x_{pl})$
	Case 2 (PNA in steel flange)	Depth of PNA	$x_{pl} = (N_{pl,a} - N_{c,f}) / (2b_f f_{y(HSS)}) + t_c$
		Ultimate moment M_{sana}	$M_{sana} = N_{c,f}(0.5h_a + h_p + 0.5h_c) + 0.5(N_{pl,a} - N_{c,f})(h_a - x_{pl} + t_c)$
	Case 3 (PNA in steel web)	Depth of PNA	$z = N_{c,f} / (2t_w f_{y(HSS)})$ $x_{pl} = 0.5h_a + t_c - z$
		Ultimate moment M_{sana}	$M_{sana} = M_{pl,a} + N_{c,f}(0.5h_a + h_p + 0.5h_c - 0.5z)$
Partial	Case 1 (PNA in steel flange)	Depth of PNA	$x_{pl} = (N_{pl,a} - N_c) / (2b_f f_{y(HSS)}) + t_c$
		Ultimate moment M_{sana}	$M_{sana} = N_c(0.5h_a + t_c - 0.5x_c) + 0.5(N_{pl,a} - N_c)(h_a - x_{pl} + t_c)$
	Case 2 (PNA in steel web)	Depth of PNA	$z = N_c / (2t_w f_{y(HSS)})$ $x_{pl} = 0.5h_a + t_c - z$
		Ultimate moment M_{sana}	$M_{sana} = M_{pl,a} + N_c(0.5h_a + t_c - 0.5x_c - 0.5z)$

Notes:

Compressive force acting on ECC $N_{c,f}$ (full shear connection): $N_{c,f} = f'_{ECC}\, b_{eff}\, h_c$

Tensile force acting on HSS $N_{pl,a}$: $N_{pl,a} = A_a f_{y(HSS)}$

Shear resistance of headed shear stud: $P_{Rd,stud} = 0.8 f_u (\pi d^2/4)/\gamma_v$

$P_{Rd,ECC} = 0.29 \alpha d^2 \sqrt{f_{ck} E_{cm}}/\gamma_v$

Compressive force acting on ECC N_c (partial shear connection): $N_c = n.\min(P_{Rd,stud}, P_{Rd,ECC})$

Height of ECC stress block (partial shear connection): $x_c = N_c/(b_{eff} f'_{ECC})$

Number of headed shear connections to assure full shear connection: $n_f = \dfrac{\min(N_{c,f}, N_{pl,a})}{\min(P_{Rd,stud}, P_{Rd,ECC})}$

Table 6
Summary of comparison of flexural strength obtained by simple and full analytical models with FE models and test results

Source	Beam group	M_{FE}/M_{sana}		M_{FE}/M_{fana}	
		Mean	SD	Mean	SD
FE models	HSS S690 beams (54 beams)	1.16	0.13	1.05	0.06
	HSS S960 beams (54 beams)	1.11	0.12	0.97	0.03
Experiment	Three tests from [18]	0.99	0.03	1.02	0.06
Overall (111 cases)		**1.13**	**0.13**	**1.01**	**0.06**

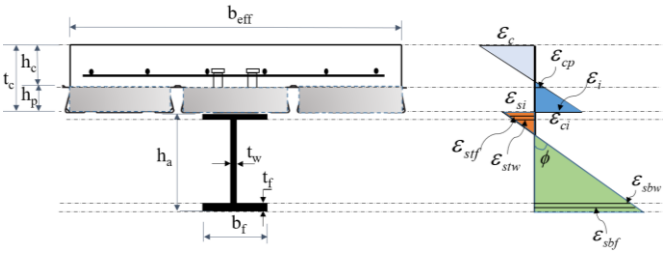

Fig. 8 Strains distributed in cross-section for full analytical model

Both full and partial shear connection are considered in this model. This analytical model is based on strain compatibility and force equilibrium of the beam's cross-section and the following assumptions were made:

(i) Strains of individual components (i.e., HSS section, ECC slab) are distributed linearly throughout the cross-section with the same curvature ϕ.

(ii) Stresses at top and bottom flanges of HSS section are constant throughout their thickness. Their values are calculated by using strains at their mid-thickness (ε_{stf} and ε_{sbf}, Fig. 8).

(iii) For slab using PSS, contribution from the ECC part in trough is ignored.

(iv) Neither plate buckling nor shear failure nor shear slag occurs.

The full analytical modelling procedure consists of four main steps and details of them are given in the following four sections.

5.1.1. Step 1: Strain distribution of the section

Strain distribution throughout the cross-section is shown in Fig. 8. The composite beam may be treated as a fully or partially shear connection by using the slip strain ε_i at the interfaces between the HSS top flange and the ECC slab such that

$$\varepsilon_i = (1-\eta)^2 \left(\frac{h_a}{2} + \frac{t_c}{2}\right)\phi \tag{2}$$

In Eqn. (2), h_a is HSS section height, t_c is the ECC slab thickness and η is the shear connection degree. In order to account for the nonlinear effect of η, slip strain is expressed as second order function of η. From Eqn. (2), for fully shear connected beam, $\eta = 1.0$ and $\varepsilon_i = 0$ (i.e., no slip between the HSS section and the ECC slab). On the other hand, if $\eta = 0$, there is no bond between the HSS section and the ECC slab so that the neutral axis of the ECC slab and HSS section will be at their corresponding mid-heights.

From Fig. 8, strains of all other components can be expressed in term of strain at the mid-thickness of HSS section's bottom flange ε_{sbf} and the beam's curvature ϕ:

$$\varepsilon_{sbw} = \varepsilon_{sbf} - \frac{t_f}{2}.\phi \tag{3}$$

$$\varepsilon_{stw} = \varepsilon_{sbf} - \left(h_a - \frac{3t_f}{2}\right).\phi \tag{4}$$

$$\varepsilon_{stf} = \varepsilon_{sbf} - \left(h_a - t_f\right).\phi \tag{5}$$

$$\varepsilon_{si} = \varepsilon_{sbf} - \left(h_a - \frac{t_f}{2}\right).\phi \tag{6}$$

$$\varepsilon_{ci} = \varepsilon_{sbf} - \left(h_a - \frac{t_f}{2}\right).\phi + \varepsilon_i \tag{7}$$

$$\varepsilon_{cp} = \varepsilon_{sbf} - \left(h_a - \frac{t_f}{2} + h_p\right).\phi + \varepsilon_i \tag{8}$$

$$\varepsilon_c = \varepsilon_{sbf} - \left(h_a - \frac{t_f}{2} + t_c\right).\phi + \varepsilon_i \tag{9}$$

In Eqns. (3) – (9), ε_{stw} and ε_{sbw} are respectively the strains at the top and bottom tips of the HSS section's web. ε_{stf} is the strain at HSS section's top flange. ε_{si} is the strain of HSS section at the interface between HSS section and ECC slab. ε_{ci} is the strain of ECC slab at the interface between HSS section and ECC slab. ε_{cp} is the strain of ECC at the tip of PSS trough while ε_c is the ECC strain at the ECC slab's top surface. t_f is the thickness of HSS section flange and h_p is the PSS trough height.

5.1.2. Steps 2: Stresses and forces of individual components

The forces acting on individual components can be calculated based on the stress distribution shown in Fig. 9. For the ECC slab, it is assumed that stress is distributed linearly throughout slab's height. As contribution from the ECC in trough is neglected, stress distribution in slab is dependent on the strain of ECC at the tip of PSS trough ε_{cp}. Based on the value of ε_{cp}, the compression force F_{cc} and tension force F_{ct} are calculated as:

$$F_{cc} = -\frac{1}{2}\sigma_c \frac{\varepsilon_c}{\phi} b_{eff} \qquad \text{if } \varepsilon_{cp} \geq 0 \tag{10}$$

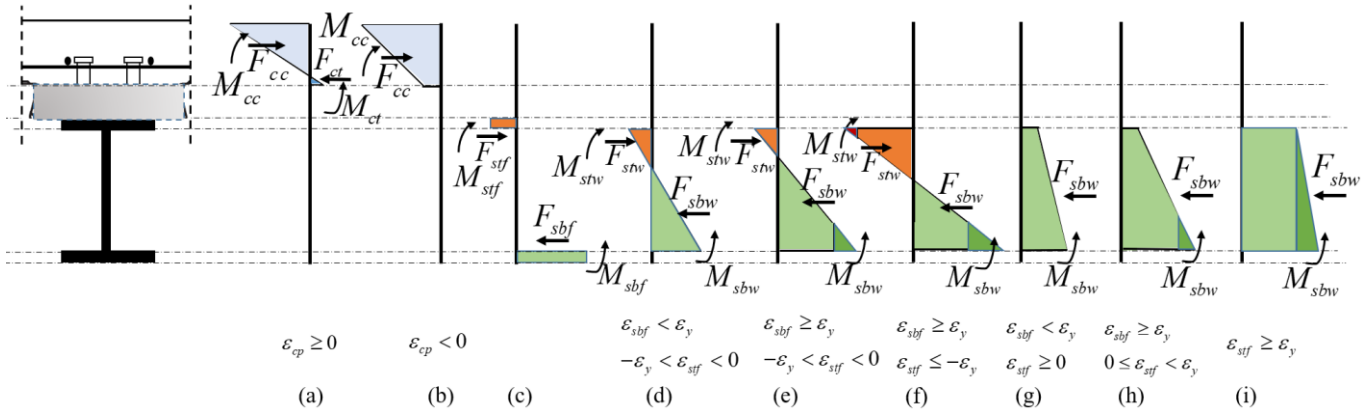

Fig. 9 Forces acting in cross-section for full analytical model

$$F_{cc} = -\frac{\sigma_c + \sigma_{cp}}{2} h_c b_{eff} \quad \text{if } \varepsilon_{cp} < 0 \tag{11}$$

$$F_{ct} = \frac{1}{2}\sigma_{cp} . \frac{\varepsilon_{cp}}{\phi} . b_{eff} \quad \text{if } \varepsilon_{cp} \geq 0 \tag{12}$$

$$F_{ct} = 0 \quad \text{if } \varepsilon_{cp} < 0 \tag{13}$$

In Eqns. (10) – (13), σ_c is the stress of ECC at the top surface of ECC slab. σ_{cp} is the stress of ECC at the tip of PSS trough. h_c is the distance from the top surface of ECC slab to the tip of PSS trough and b_{eff} is the effective width of ECC slab. For composite beam using solid slab, in Eqns. (10) – (13), ε_{cp} is replaced by the strain at the bottom of ECC slab ε_{ci} while σ_{cp} is replaced by σ_{ci}.

All stress terms used in Eqns. (10) – (13) can be calculated based on the stress – strain model of ECC shown in Figs. 2(e) and (f) by using the following equations:

For ECC in compression (Fig. 2(e)):

$$\sigma_c = \begin{cases} f'_c \frac{\varepsilon_c}{\varepsilon_{co}} \left\{ 0.8 \left(1 - \frac{\varepsilon_c}{\varepsilon_{co}} \right) + 1 \right\} & 0 \leq \varepsilon_c \leq \varepsilon_{co} \\ f'_c + \frac{(\sigma_l - f'_c)(\varepsilon_c - \varepsilon_{co})}{\varepsilon_l - \varepsilon_{co}} & \varepsilon_{co} < \varepsilon_c \leq \varepsilon_l \end{cases} \tag{14}$$

For ECC in tension (Fig. 2(f)):

$$\sigma_t = \begin{cases} \frac{f_t}{\varepsilon_{t0}} \varepsilon_t & 0 \leq \varepsilon_t \leq \varepsilon_{t0} \\ \sigma_{tp} + \frac{(\sigma_{tp} - f_t)(\varepsilon_t - \varepsilon_{t0})}{\varepsilon_{tp} - \varepsilon_{t0}} & \varepsilon_{t0} < \varepsilon_t \leq \varepsilon_{tp} \end{cases} \tag{15}$$

Forces acting on top and bottom steel flanges are then calculated by using Eqns. (16)-(17):

$$F_{sbf} = \sigma_{sbf} . b_f . t_f \tag{16}$$

$$F_{stf} = \sigma_{stf} . b_f . t_f \tag{17}$$

Forces acting on the top and bottom of steel web can be obtained by using Eqns. (18)-(25):

$$F_{sbw} = \frac{\sigma_{sbw} . \varepsilon_{sbw} . t_w}{2\phi} \quad \text{if } \varepsilon_{sbw} < \varepsilon_y \ \& \ -\varepsilon_y < \varepsilon_{stw} < 0 \tag{18}$$

$$F_{sbw} = \left(\frac{f_y \left(\varepsilon_{sbw} - \frac{\varepsilon_y}{2} \right)}{\phi} + \frac{1}{2} \frac{(\sigma_{sbw} - f_y)(\varepsilon_{sbw} - \varepsilon_y)}{\phi} \right) t_w \quad \text{if } \varepsilon_{sbw} \geq \varepsilon_y \ \& \ \varepsilon_{stw} < 0 \tag{19}$$

$$F_{sbw} = \frac{1}{2} (\sigma_{sbw} + \sigma_{stw}) (h_a - 2t_f) t_w \quad \text{if } \varepsilon_{sbw} < \varepsilon_y \ \& \ \varepsilon_{stw} \geq 0 \tag{20}$$

$$F_{sbw} = \left(\frac{f_y \left(\varepsilon_{sbw} - \frac{\varepsilon_y}{2} \right) - \frac{1}{2} \sigma_{stw} . \varepsilon_{stw}}{\phi} + \frac{1}{2} \frac{(\sigma_{sbw} - f_y)(\varepsilon_{sbw} - \varepsilon_y)}{\phi} \right) t_w \quad \text{if } \varepsilon_{sbw} \geq \varepsilon_y \ \& \ 0 \leq \varepsilon_{stw} < \varepsilon_y \tag{21}$$

$$F_{sbw} = \left(\sigma_{stw} + \frac{1}{2} (\sigma_{sbw} - \sigma_{stw}) \right) (h_a - 2t_f) t_w \quad \text{if } \varepsilon_{stw} \geq \varepsilon_y \tag{22}$$

$$F_{stw} = \left(\frac{f_y \left(\varepsilon_{stw} + \frac{\varepsilon_y}{2} \right)}{\phi} - \frac{1}{2} \frac{(\sigma_{stw} + f_y)(\varepsilon_{sbw} + \varepsilon_y)}{\phi} \right) t_w \quad \text{if } \varepsilon_{stw} \leq -\varepsilon_y \tag{23}$$

$$F_{stw} = -\frac{\sigma_{stw} . \varepsilon_{stw} . t_w}{2\phi} \quad \text{if } -\varepsilon_y < \varepsilon_{stw} < 0 \tag{24}$$

$$F_{stw} = 0 \quad \text{if } \varepsilon_{stw} \geq 0 \tag{25}$$

All stresses terms used in Eqns. (18) to (25) can be calculated using constitutive model of HSS shown in Fig. 2(a) which can be expressed as:

$$\sigma_s = \begin{cases} E_s.\varepsilon_s & \varepsilon_s \le \varepsilon_y \\ f_y + \dfrac{\left(\varepsilon_s - \varepsilon_y\right)\left(f_u - f_y\right)}{\varepsilon_u - \varepsilon_y} & \varepsilon_y < \varepsilon_s \le \varepsilon_u \end{cases} \tag{26}$$

5.1.3. Step 3: Forces equilibrium for the solution of ϕ and moment calculation

If the beam is under bending only, applying compressive and tension forces equilibrium of the cross-section implies that:

$$F_{cc} + F_{stf} + F_{stw} = F_{ct} + F_{sbw} + F_{sbf} \tag{27}$$

For any given value of ε_{sbf} which defines the strain status of the section (Eqns. (3) to (9)), Eqn. (27) is obviously a nonlinear equation for the solution of the beam's curvature ϕ. For a given value of ε_{sbf}, by starting with reasonable lower and upper estimates of ϕ, a converged solution of ϕ (i.e., corresponding to an error tolerance of 0.01% of the unbalance force) can be obtained by the standard bi-section method using MATLAB.

After the value ϕ is solved from Eqn. (27), by referring to Fig. 9 again, moment contributions from different components about the mid-thickness of the bottom flange of steel section at different stages of the beam can be calculated by using Eqns. (28) – (41).

$$M_{sbf} = 0 \tag{28}$$

$$M_{stf} = \sigma_{stf}.b_f.t_f.\left(h_a - t_f\right) \tag{29}$$

$$M_{sbw} = \frac{\sigma_{sbw}.\varepsilon_{sbw}.t_w}{2\phi}\left(\frac{\varepsilon_{sbw}}{3\phi} + \frac{t_f}{2}\right) \quad \text{if} \quad \varepsilon_{sbw} < \varepsilon_y \;\&\; -\varepsilon_y < \varepsilon_{stw} < 0 \tag{30}$$

$$M_{sbw} = \frac{f_y\left(\varepsilon_{sbw} - \varepsilon_y\right)t_w}{\phi}\left(\frac{\varepsilon_{sbw} - \varepsilon_y}{2\phi} + \frac{t_f}{2}\right) + \frac{f_y.\varepsilon_y.t_w}{2\phi}\left(\frac{3\varepsilon_{sbw} - 2\varepsilon_y}{3\phi} + \frac{t_f}{2}\right) + \frac{1}{2}\frac{\left(\sigma_{sbw} - f_y\right)\left(\varepsilon_{sbw} - \varepsilon_y\right)t_w}{\phi}\left(\frac{\varepsilon_{sbw} - \varepsilon_y}{3\phi} + \frac{t_f}{2}\right) \quad \text{if} \quad \varepsilon_{sbw} \ge \varepsilon_y \;\&\; \varepsilon_{stw} < 0 \tag{31}$$

$$M_{sbw} = \sigma_{stw}\left(h_a - 2t_f\right)t_w\left(\frac{h_a - t_f}{2}\right) + \frac{1}{2}\left(\sigma_{sbw} - \sigma_{stw}\right)\left(h_a - 2t_f\right)t_w\left(\frac{2h_a - t_f}{6}\right) \quad \text{if} \quad \varepsilon_{sbw} < \varepsilon_y \;\&\; \varepsilon_{stw} \ge 0 \tag{32}$$

$$M_{sbw} = \frac{f_y\left(\varepsilon_{sbw} - \varepsilon_y\right)t_w}{\phi}\left(\frac{\varepsilon_{sbw} - \varepsilon_y}{2\phi} + \frac{t_f}{2}\right) + \frac{f_y.\varepsilon_y.t_w}{2\phi}\left(\frac{3\varepsilon_{sbw} - 2\varepsilon_y}{3\phi} + \frac{t_f}{2}\right) - \frac{\sigma_{stw}.t_w.\varepsilon_{stw}}{2\phi}\left(\frac{\varepsilon_{stw}}{3\phi} + h_a - \frac{3t_f}{2}\right) + \frac{1}{2}\frac{\left(\sigma_{sbw} - f_y\right)\left(\varepsilon_{sbw} - \varepsilon_y\right)t_w}{\phi}\left(\frac{\varepsilon_{sbw} - \varepsilon_y}{3\phi} + \frac{t_f}{2}\right) \quad \text{if} \quad \varepsilon_{sbw} \ge \varepsilon_y \;\&\; 0 \le \varepsilon_{stw} < \varepsilon_y \tag{33}$$

$$M_{sbw} = \sigma_{stw}\left(h_a - 2t_f\right)t_w\left(\frac{h_a - t_f}{2}\right) + \frac{1}{2}\left(\sigma_{sbw} - \sigma_{stw}\right)\left(h_a - 2t_f\right)t_w\left(\frac{2h_a - t_f}{6}\right) \quad \text{if} \quad \varepsilon_{stw} \ge \varepsilon_y \tag{34}$$

$$M_{stw} = \frac{\sigma_{stw}.\varepsilon_{stw}.t_w}{2\phi}\left(h_a - \frac{3t_f}{2} - \frac{\varepsilon_{stw}}{3\phi}\right) \quad \text{if} \quad -\varepsilon_y < \varepsilon_{stw} < 0 \tag{35}$$

$$M_{stw} = -\frac{f_y\left(\varepsilon_{stw} + \varepsilon_y\right)t_w}{\phi}\left(h_a - \frac{3t_f}{2} + \frac{\varepsilon_{stw} - \varepsilon_y}{2\phi}\right) + \frac{f_y.\varepsilon_y.t_w}{2\phi}\left(h_a - \frac{3t_f}{2} + \frac{3\varepsilon_{stw} - 4\varepsilon_y}{3\phi}\right) + \frac{1}{2}\frac{\left(\sigma_{stw} + f_y\right)\left(\varepsilon_{stw} + \varepsilon_y\right)t_w}{\phi}\left(h_a - \frac{3t_f}{2} + \frac{\varepsilon_{stw} + \varepsilon_y}{3\phi}\right) \quad \text{If} \quad \varepsilon_{stw} \le -\varepsilon_y \tag{36}$$

$$M_{stw} = 0 \quad \text{if} \quad \varepsilon_{stw} \ge 0 \tag{37}$$

$$M_{cc} = \frac{\sigma_c.\varepsilon_c.b_{eff}}{2\phi}\left(h_a + t_c - \frac{t_f}{2} + \frac{\varepsilon_c}{3\phi}\right) \quad \text{if} \quad \varepsilon_{cp} \ge 0 \tag{38}$$

$$M_{cc} = \frac{\sigma_{cp}\left(\varepsilon_c - \varepsilon_{cp}\right)}{\phi}\left(h_a + t_c - \frac{t_f}{2} + \frac{\varepsilon_c - \varepsilon_{cp}}{\phi}\right)b_{eff} + \frac{\left(\sigma_c - \sigma_{cp}\right)\left(\varepsilon_c - \varepsilon_{cp}\right)b_{eff}}{2\phi}\left(h_a + t_c - \frac{t_f}{2} + \frac{\varepsilon_c - \varepsilon_{cp}}{3\phi}\right) \quad \text{if} \quad \varepsilon_{cp} < 0 \tag{39}$$

$$M_{ct} = \frac{\sigma_{cp}.\varepsilon_{cp}.b_{eff}}{2\phi}\left(h_a + h_p - \frac{t_f}{2} + \frac{\varepsilon_{cp}}{3\phi}\right) \quad \text{if} \quad \varepsilon_{cp} \geq 0 \tag{40}$$

$$M_{ct} = 0 \quad \text{if} \quad \varepsilon_{cp} < 0 \tag{41}$$

It should be noted that if solid slab is used instead of PSS, in Eqns. (39)-(41), ε_{cp} and σ_{cp} should be replaced by ε_{ci} and σ_{ci}, respectively.

5.1.4. Step 4: Effective stiffness and deflection calculation

After the moment contribution is known, internal moment in the cross-section can be calculated as:

$$M_{f\,ana} = M_{sbf} - M_{stf} + M_{sbw} - M_{stw} - M_{cc} + M_{ct} \tag{42}$$

Beam's effective bending stiffness EI_{eff} can be achieved as:

$$EI_{eff} = \frac{M_{f\,ana}}{\phi} \tag{43}$$

And the mid-span deflection δ_{max} for the beam under four-point bending can be obtained as:

$$P_{f\,ana} = \frac{M_{f\,ana}}{a} \tag{44}$$

$$\delta_{max} = \frac{P_{f\,ana}\,a\left(3L^2 - 4a^2\right)}{24EI_{eff}} \tag{45}$$

In Eqns. (44) and (45), P_{fana} is the loading corresponding to M_{fana} and a is the shear span of the beam. Obviously, expression of Eqn. (45) can be modified for other loading cases easily. In order to trace out the entire load-deformation curve, an incremental procedure is employed by starting from an initial value of $\varepsilon_{sbf} = 0$ (so that $P_{fana}=0$ and $\delta_{max}=0$). A small increment of ε_{sbf} (i.e., 0.02%) is applied incrementally so that the above four-step procedure are repeatedly applied to obtain the corresponding load and deflection.

5.2. Validation of the full analytical model

The full analytical model was validated against experimental results obtained from the three ECC-HSS composite beams (ECC40-140, ECC-70-140, ECC-40-170) tested by the authors [18]. The flexural strengths obtained from full analytical model of the three beams tested are compared against the test results in Fig. 10(a) which shows a good agreement between the analytical model and the test results. In terms of load – displacement curves, Figs. 10(b)-(d) show that the full analytical model captured the behaviours of the tested beams at different stages with the results similar to the test and FE results..

In order to further validate the accuracy and reliability of the proposed full analytical model, it was employed to predict the flexural strengths and load-deflection curves of all the 108 models generated using FE model. Examples of some selected load-deflection curve comparisons are shown in Fig. 11 for the configuration SW600-ST140-ID180 using PSS with different material properties. Fig. 11 shows that the analytical and the FE model curves are well agreed with each other. Results from another comparison example for the same configuration with solid slab are shown in Fig. 12. Furthermore, results of beams with different HSS section depths, slab thicknesses are compared in Figs. 13(a) and (b), respectively. Figs. 12 and 13 again indicate that the proposed full analytical model was able to predict the load-displacement relationship of the beams with good accuracy.

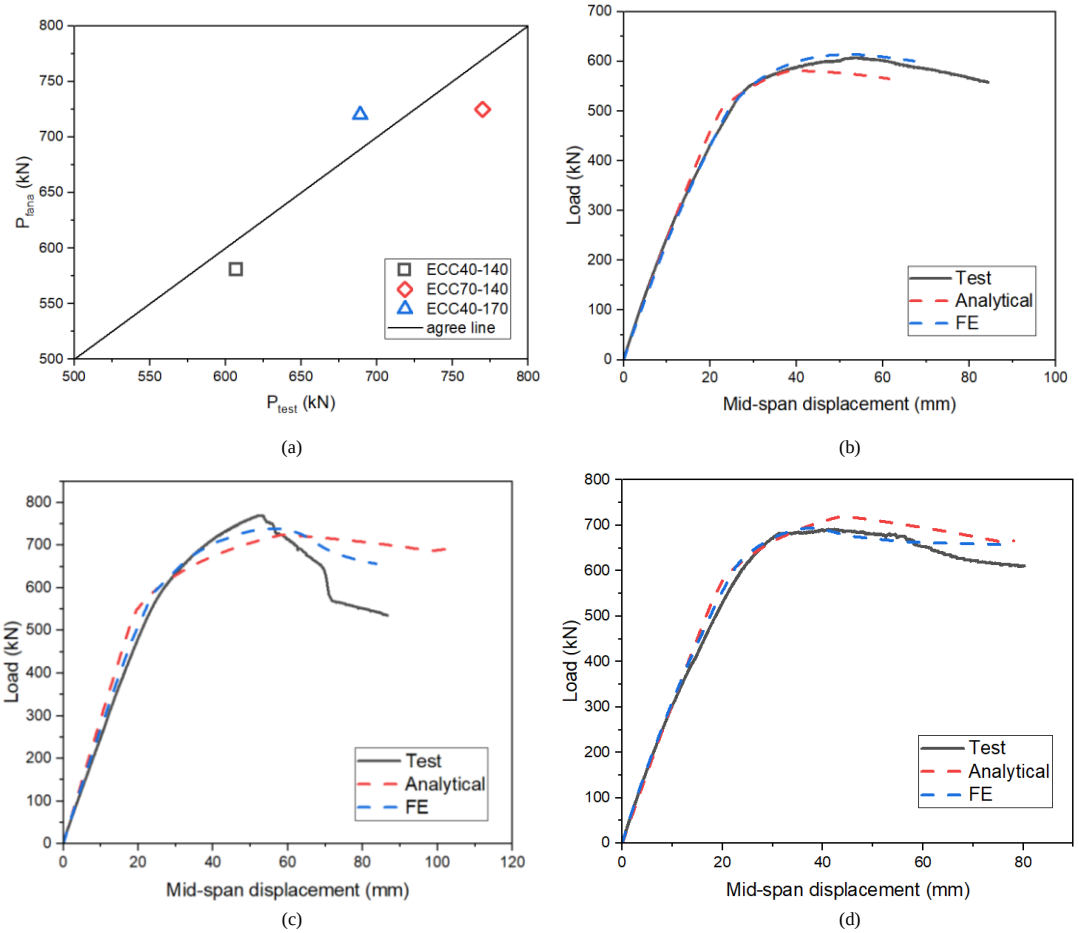

Fig. 10 Results obtained from full analytical model compared with tests and FE results in [18]: (a) Comparison of the test and full analytical model in terms of flexural strength; (b) Load – displacement curves of beam ECC40-140; (c) Load – displacement curves of beam ECC70-140; (d) Load – displacement curves of beam ECC40-170

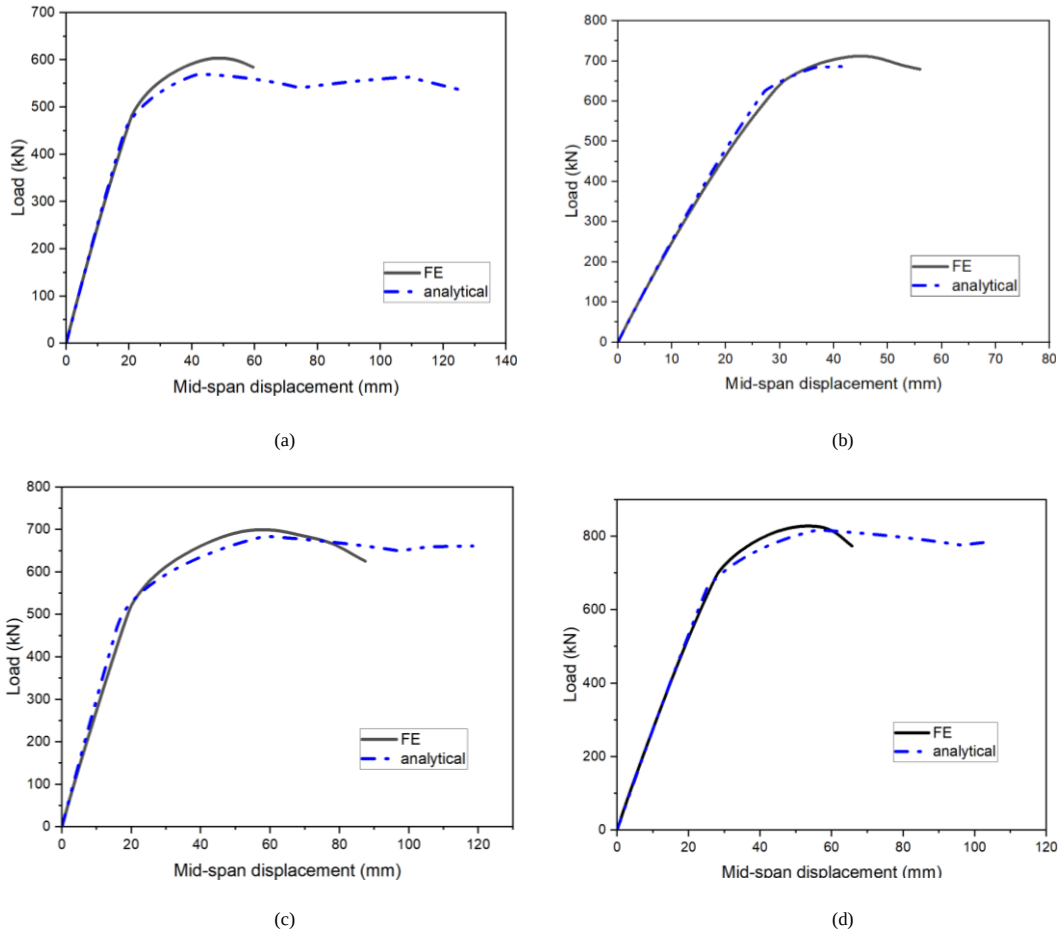

Fig. 11 Full analytical model results of beam SW600-ST140-ID180 using PSS with different material properties compared with FE model results. (a) E40-S690; (b) E40-S960; (c) E70-S690; (d) E70-S960

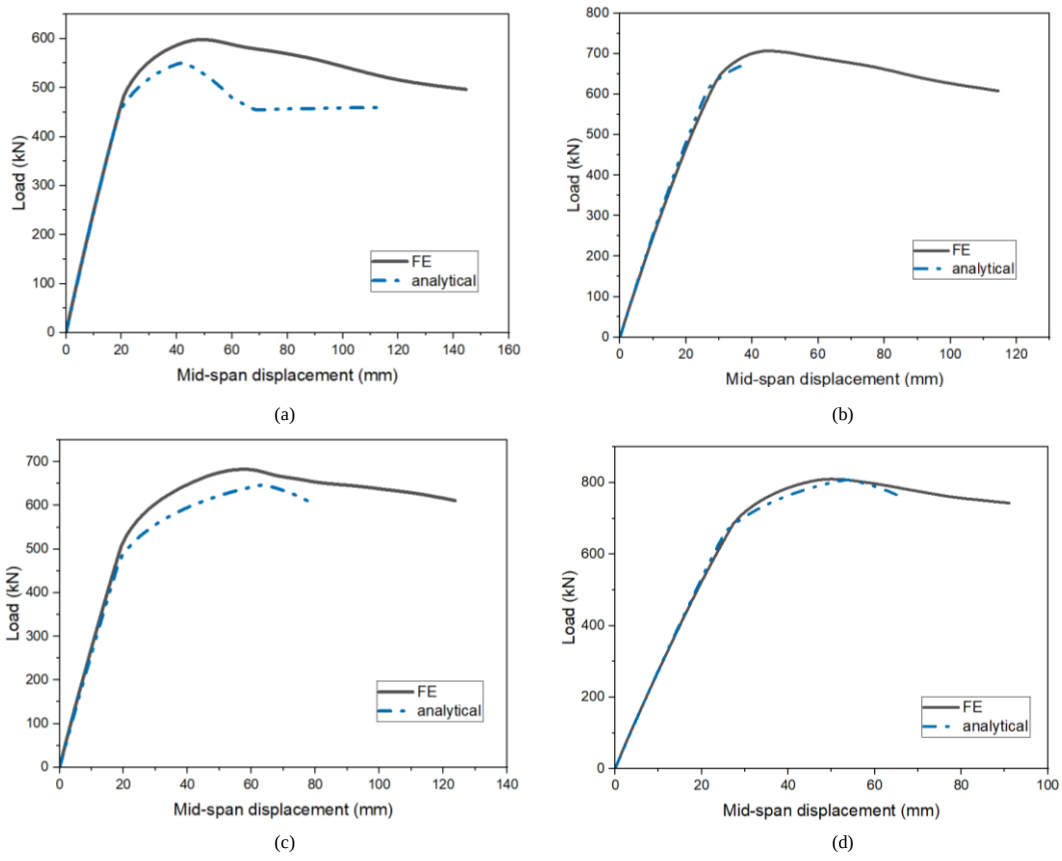

Fig. 12 Full analytical model results of beam SW600-ST140-ID180 using solid slab compared with FE model results: (a) E40-S690; (b) E40-S960; (c) E70-S690; (d) E70-S960

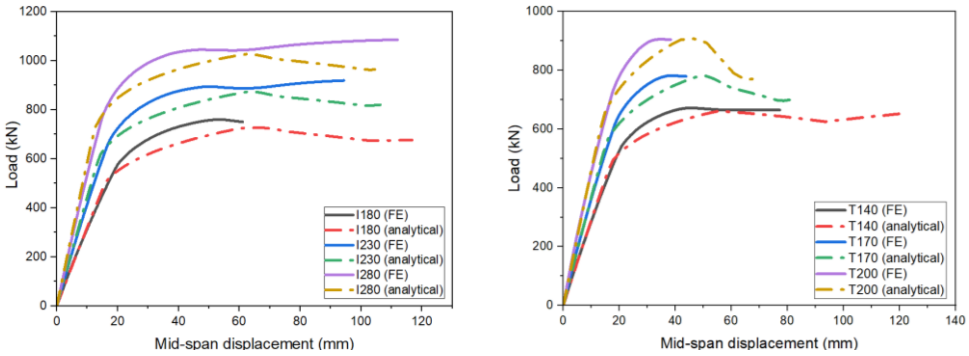

Fig. 13 Full analytical model results of different beams compared with FE model results: (a) Beams with different HSS section depths; (b) Beams with different slab thickness

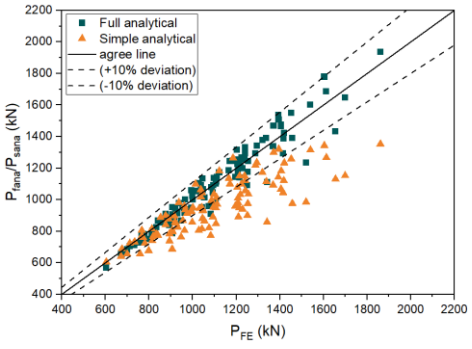

Fig. 14 Flexural strength obtained by full and simple analytical models compared with FE models

Regarding flexural strength prediction, comparisons between the simple analytical model and the full analytical model against the FE modelling results for all 108 models are plotted in Fig. 14. Fig. 14 shows that virtually all full analytical model results are within the 10% deviation lines. On the other hand, predictions by the simple analytical model have a wider scattering and generally underpredict the flexural strength. The mean and standard deviation of flexural strength prediction ratios obtained by the simple analytical model (M_{sana}) and the full analytical models (M_{fana}) for the three tested beams in [18] and the 108 FE models (M_{FE}) are summarized in Table 6. Table 6 clearly shows that the full analytical model results are more accurate and reliable than the simple analytical model results.

6. Conclusions

In this study, by using a validated 3D finite element (FE) model developed in authors' previous work [18], 108 models were generated and analysed to assess the accuracies of RPA approaches in predicting the flexural capacity of ECC-HSS composite beams. Simple and full analytical models were also developed in order to obtain the bending responses of these beams. Based on the results achieved, the following conclusions can be drawn.

(1) It is found that RPA approaches underpredicted (on average from 17% to 38%) the flexural strength of the ECC-HSS composite beams. Hence, an improved simple analytical model accounting for the higher compressive ductility of ECC was proposed. Validation with experimental and FE modelling results found that this simple analytical model produced more accurate predictions and reduced the average underprediction to 13%.

(2) In order to produce the full load-deflection curve of the beams without running any time-consuming FE model, full analytical model that is based on strain compatibility and force equilibrium was developed and validated against experimental and FE model results. Validation results show that this full analytical model produced more accurate and reliable results than the simple analytical model with prediction accuracy very close to the 3D FE modelling and tests results.

Acknowledgment

University International Postgraduate Award (UIPA) provided by UNSW Sydney for the first author to pursue his PhD are gratefully acknowledged.

This work was supported by The University of Danang, University of Science and Technology, code number of Project: T2023-02-11.

References

[1] Shi, G., et al., Local buckling of 460 MPa high strength steel welded section stub columns under axial compression. Journal of Constructional Steel Research, 2014. 100: p. 60-70.
[2] Shi, G., H. Ban, and F.S.K. Bijlaard, Tests and numerical study of ultra-high strength steel columns with end restraints. Journal of Constructional Steel Research, 2012. 70: p. 236-247.
[3] Shi, G., W. Zhou, and C. Lin, Experimental investigation on the local buckling behavior of 960 MPa high strength steel welded section stub columns. Advances in Structural Engineering, 2015. 18.
[4] Shi, G., et al., Local buckling behavior of welded stub columns with normal and high strength steels. Journal of Constructional Steel Research, 2016. 119: p. 144-153.
[5] Ban, H., et al., Experimental investigation of the overall buckling behaviour of 960MPa high strength steel columns. Journal of Constructional Steel Research, 2013. 88: p. 256-266.
[6] Rasmussen, K. and G. Hancock, Tests of high strength steel columns. Journal of Constructional Steel Research, 1995. 34: p. 27–52.
[7] Lee, C.-H., et al., Flexural strength and rotation capacity of I-shaped beams fabricated from 800-MPa steel. Journal of Structural Engineering, 2013. 139(6): p. 1043-1058.
[8] Joo, H.S., et al., Rotational capacity and optimum bracing point of high strength steel I-girders. Journal of Constructional Steel Research, 2013. 88: p. 79-89.
[9] Uy, B., Stability and ductility of high performance steel sections with concrete infill. Journal of Constructional Steel Research, 2008. 64(7-8): p. 748-754.
[10] Kim, C.-S., et al., Eccentric axial load capacity of high-strength steel-concrete composite columns of various sectional shapes. Journal of Structural Engineering, 2014. 140(4): p. 04013091.
[11] Khan, M.K.I., et al., Behaviour of engineered cementitious composite-encased stub concrete columns under axial compression. Magazine of Concrete Research, 2020. 72(19): p. 984-1005.
[12] Puthli, R. and O. Fleischer, Investigations on bolted connections for high strength steel members. Journal of constructional steel research, 2001. 57(3): p. 313-326.
[13] Može, P. and D. Beg, Investigation of high strength steel connections with several bolts in double shear. Journal of constructional steel research, 2011. 67(3): p. 333-347.
[14] Coelho, A.M.G. and F.S. Bijlaard, Experimental behaviour of high strength steel end-plate connections. Journal of Constructional Steel Research, 2007. 63(9): p. 1228-1240.
[15] Elghazouli, A. and J. Treadway, Inelastic behaviour of composite members under combined bending and axial loading. Journal of Constructional Steel Research, 2008. 64(9): p. 1008-1019.
[16] Kabir, M.I., et al., Flexural behaviour of ECC-LWC encased slender high strength steel composite beams. Journal of Constructional Steel Research, 2020. 173: p. 106253.
[17] Kabir, M.I., et al., Flexural behaviour of engineered cementitious composite encased high strength steel composite beam. ce/papers, 2019. 3(3-4): p. 713-718.
[18] Cong-Luyen Nguyen and C.K. Lee, Flexural behaviours of Engineered Cementitious Composites – High strength steel composite beams. Engineering Structures, 2021. 249.
[19] Uy, B. and R. Sloane, Behavior of composite tee beams constructed with high strength steel. Journal of Constructional Steel Research, 1998. 1: p. 203-4.
[20] Zhao, H. and Y. Yuan, Experimental studies on composite beams with high-strength steel and concrete. Steel and Composite Structures, 2010. 10(5): p. 373-383.
[21] Ban, H. and M.A. Bradford, Flexural behaviour of composite beams with high strength steel. Engineering Structures, 2013. 56: p. 1130-1141.
[22] Ban, H., et al., Available rotation capacity of composite beams with high-strength materials under sagging moment. Journal of Constructional Steel Research, 2016. 118: p. 156-168.
[23] Shamass, R. and K.A. Cashell, Behaviour of Composite Beams Made Using High Strength Steel. Structures, 2017. 12: p. 88-101.
[24] Ban, H. and M.A. Bradford, Elastoplastic cross-sectional behavior of composite beams with high-strength steel: analytical modeling. Journal of Structural Engineering, 2015. 141(10): p. 04014236.
[25] EN 1994-1-1:2004 Eurocode 4: Design of Composite Steel and Concrete Structures Part 1-1: General rules and Rules for Buildings.
[26] Standards Australia. AS 2737.1-2003. Composite Structures Part 1: Simply supported beams. Sydney: Standards Australia, 2003.
[27] Li, V.C., Engineered Cementitious Composites (ECC): Bendable Concrete for Sustainable and Resilient Infrastructure. 2019: Springer.
[28] Meng, D., et al., Mechanical behaviour of a polyvinyl alcohol fibre reinforced engineered cementitious composite (PVA-ECC) using local ingredients. Construction and Building Materials, 2017. 141: p. 259-270.
[29] Cong-Luyen Nguyen, C.K.Lee, Experimental study of flexural behaviour of high strength steel (HSS)-Engineered Cementitious Composites (ECC) composite beam with profiled steel sheeting. ce/papers, 2021. 4(2-4): p. 781-786.
[30] Abaqus, V., 6.14-1. Abaqus/standard user's manual and Abaqus CAE manual. Providence, RI, USA: Dassault Systemes Simulia Corp, 2014.
[31] Oehlers, D.J. and M.A. Bradford, Composite steel and concrete structures: fundamental behaviour: fundamental behaviour. 2013: Elsevier.